Identifying Sets of Favorable Projections for Few-View Low-Dose Cone-Beam CT Scanning

Ziyi Zheng and Klaus Mueller

***Abstract*— Cone-beam computed tomography is beginning to emerge as a widely used technique for medical imaging. However, here has been growing concerns with regards to the X-ray dose delivered to the patient. Low dose CT has thus been gaining substantial interest. It can be achieved by lowering the X-ray dose per projection and/or reducing the number of projections acquired. In this work we focus on the latter and provide some new insight on how to identify favorable (or salient) views that maximize the information used within an iterative reconstruction framework. Based on prior knowledge on the object to be scanned, we propose an optimization framework that can automatically identify a minimal set of projections that can capture the salient object features. Our results indicate that these generalized views result in better image quality than evenly distributed projections.**

***Index Terms*—Iterative CT, low-dose CT, view optimization**

I. Introduction

Cone-beam CT has emerged as a major X-ray imaging modality both in terms of image quality and scan time. A popular cone-beam CT reconstruction method is the FDK [1] algorithm, which provides high resolution results but requires several hundreds of patient X-ray projections. With the growing concern about the potential risk of X-ray radiation exposure to the human body, dose reduction in cone-beam scanning (and other modalities) has become a significant research topic. Dose reduction usually involves lowering the X-ray energy per projection and/or reducing the total number of projections. Both methods typically suffer from low signal-to-noise ratio (SNR) in the reconstructions. Iterative reconstruction schemes, matched with suitable regularization methods were shown to cope well with these few-view or high-noise scenarios [2][3][4].

The work presented here focuses on one specific low-dose CT measure: reducing the number of projections. It capitalizes on the fact that in standard radiography physicians and X-ray technologists typically have a good idea, often based on standards, at what patient orientation the radiograph should be taken to reveal the desired insight. We denote these views as *salient views*. We propose to formalize and generalize the concept of salient views for CT reconstruction, and use iterative CT reconstruction to cope with the potentially irregular and sparse view distribution. To identify the salient views we analyze prior reconstructions, locate the salient features, and determine the projection(s) at which these features differentiate best. Once the salient views are obtained, we use a set-covering framework to accelerate the search for the optimal scanning configuration and trajectory that covers all of these views.

Ziyi Zheng and Klaus Mueller are with the Computer Science Department, Stony brook University, Stony Brook, NY 11777 USA (phone: 631-632-1524; e-mail: {zizhen, mueller}@ cs.sunysb.edu).

Our paper is organized as follows. Section 2 discusses related work. Section 3 describes our framework. Section 4 presents some initial results, and Section 5 ends with conclusions.

II. Related Work

In iterative reconstruction algorithms, the volume voxels represent the unknown variables and the projection pixels represent the known variables. Algebraic techniques formulate the reconstruction problem as solving a linear system. However, in the few view case, this linear system may be underdetermined. There will be many plausible solutions which make it difficult to converge to the true solution. This implies a lower bound on the number of projections. Herman and Davidi [6] demonstrated that in the few-view case, a reconstruction algorithm can generate misleading results. Sorzano et al. [5] showed that some evenly distributed overabundant views were crucial to help the few-view case. Recently, regularization methods [2][3][4] have been proposed to help iterative reconstruction in few projection case and they were able to generate very promising results .

Scott et al. [7] present methods for view planning with visible light. They show that based on prior knowledge, some views are more important because they can capture salient information about the object, while other views have less pronounced effects. The optimal placement of cameras – in our case X-ray source-detector pairs – is known to be NP-hard. Hence, we propose a set-covering problem formulation in our framework.

III. Approach

The central underlying theory to the optimal X-ray view selection problem we propose is that in the context of CT, a sharp discontinuity (an edge) can only be reliably reconstructed (from the projection data alone) if some X-ray in some of the projections is tangent to this curve [8]. We can determine these edges from prior information, typically existing scans or atlases. Once these salient rays are identified, we use the set-covering algorithm to find the set of views that contain them, and perform CT reconstruction via an iterative scheme.

A. Feature parameterization

The Radon transform is the fundamental concept in CT. The 2D Radon transform represents an object in terms of its line integrals (projections). Its continuous 2D Radon transform is:

$$Rf(t,\varphi) = \int_{-\infty}^{+\infty} f(t\cos\varphi - s\sin\varphi, t\sin\varphi + s\cos\varphi)ds \qquad (1)$$

where t is the distance of the line from the origin and φ is the angle of the normal of the line with the x-axis and $\varphi \in [0,\pi)$. Equation (1) can be reformulated as a 2D integral:

$$Rf(t,\varphi) = \int_{-\infty}^{+\infty}\int_{-\infty}^{+\infty} f(x,y)\delta(p)dxdy \qquad (2)$$

where $$p = x\cos\varphi + y\sin\varphi - t \qquad (3)$$

The Radon transform defined in equations (2, 3) is similar to the Hough transform which is well known for the detection of lines. It can be proven that these two transforms are equivalent [9]. We have used the Hough transforms representation since it is more convenient to compute its discrete form.

In the prior 2D data, we define edges as features that need to be covered by projections. To parameterize edges, we apply the Hough transform to the gradient image ∇f rather than the original image f. Then each gradient represents the normal $\mathbf{n} = (n_x, n_y)$ of a 2D edge. The updated equation is:

$$Rf'(t,\varphi) = \int_{-\infty}^{+\infty}\int_{-\infty}^{+\infty} |\nabla(f(x,y))|\,\delta(p)dxdy \qquad (4)$$

$$p = xn_x + yn_y - t \qquad (5)$$

Equation (4, 5) can be approximated by discrete integration. Fig 1(a) shows an example: a collection of geometrical primitives. A point cluster in (c) is due to a 2D line in (a). The intensity of a point in this feature space is defined by computing $Rf'(t,\varphi)$. Finally, (b) is a reconstruction using views due to the 8 major clusters and 5 further views.

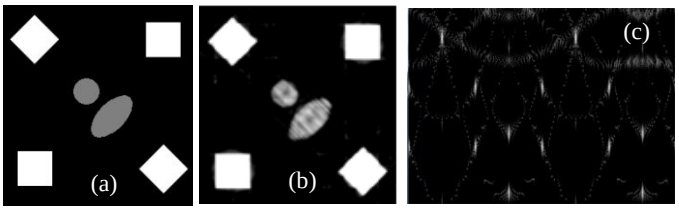

Figure 1: Reconstruction from optimal views. (a) Phantom. (b) Reconstruction from 8 salient and 5 extra views. (c) Hough transform of the edge image.

Next, we generalize the edge-based feature space to 3D. In 3D space, edges generalize to small iso-value planes and we define these planes as features. Whether the plane normal is positive or negative is irrelevant. Then we end up with two parameters. One is the normal of the iso-value plane, the other the signed distance to the origin. The 3D Radon transform, similar to the 3D Hough transform, is defined using the integral of a 3D plane. Given a plane with normal $\mathbf{n}$ and the signed distance to the origin, t, the 3D continuous Radon transform is:

$$Rf(t,\mathbf{n}) = \int_{-\infty}^{+\infty}\int_{-\infty}^{+\infty}\int_{-\infty}^{+\infty} f(x,y,z)\delta(p_3)dxdydz \qquad (6)$$

where $$p_3 = Ax + By + Cz + D \qquad (7)$$

Equation (7) denotes a 3D plane defined by $\mathbf{n}$ and t. The signed distance from origin to plane in (7) is:

$$t = \frac{A\cdot 0 + B\cdot 0 + C\cdot 0 + D}{\sqrt{A^2+B^2+C^2}} = \frac{D}{\sqrt{A^2+B^2+C^2}} \qquad (8)$$

Then the plane that goes through a given point (x_0, y_0, z_0) with normal (n_x, n_y, n_z) is defined as:

$$n_x(x-x_0) + n_y(y-y_0) + n_z(z-z_0) = 0 \qquad (9)$$

There exists a unique vector $\mathbf{p}$ whose vector field will define the normal of the plane and whose length will indicate the location of the plane starting from the origin (see Fig. 2):

$$\mathbf{p} = t\cdot\frac{\mathbf{n}}{|\mathbf{n}|} = \frac{D}{\sqrt{A^2+B^2+C^2}}\cdot\frac{(n_x,n_y,n_z)}{\sqrt{n_x^2+n_y^2+n_z^2}} = \frac{n_x x_0 + n_y y_0 + n_z z_0}{n_x^2+n_y^2+n_z^2}(n_x,n_y,n_z) \qquad (10)$$

Thus we can merge the two parameters $\mathbf{n}$ and t into a single 3D point $\mathbf{p}$. This point $\mathbf{p}$ is on the integration plane and at the shortest distance from the origin to the plane. Fig. 3 shows a simple example. Assume we know the object to be scanned (here a simple square object) and roughly know its extent and position (Fig. 3a). We first take the gradient image (Fig 3b). By performing discrete integration based on equations (6, 7, 10),

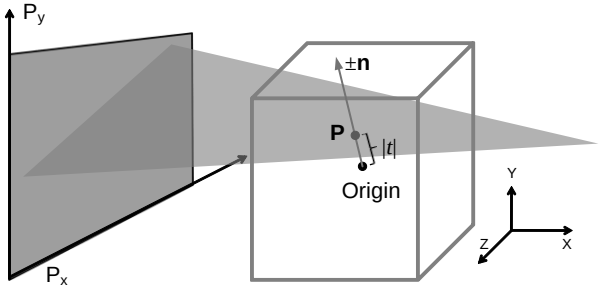

Figure 2. 3D plane parameterization

we get plane-point pairs in 3D space (Fig. 3c). These *planes* are the image-space equivalents to the *points* in the Hough transform. We can cluster in either domain, but we prefer to cluster in the image domain since we observe better spatial coherence there. Next, we use thresholding to reduce the noise, which will leave only high intensity planes, as shown in Fig. 3d.

The discrete computation can be noisy. Furthermore, in the clinical case, the planes are usually not as strong as in this phantom case. To get better feature extraction in noisy cases, we apply k-means clustering [10] to extract features.

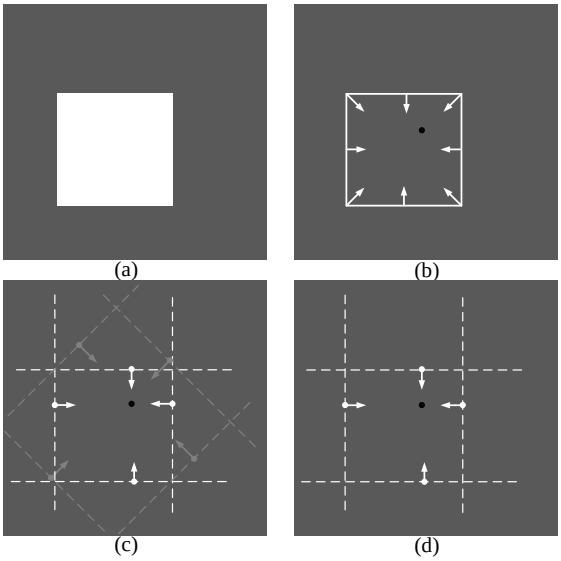

Figure 3. (a) shows the prior volume, (b) shows the gradient with arrows indicating direction and intensity indicating strength, (c) shows the plane detection and the unique points to represent planes. (d) shows the planes after thresholding. The black dot is the origin.

B. Set-Cover Problem

After extracting the prominent edges, we optimize the view positions to cover these features. The overall mindset behind our method is that if there are no rays to cover the strong edges, then it will be difficult for a reconstruction algorithm to produce them and for a (later) regularization method to restore them.

We reformulate the dose minimization problem into the well-studied set-cover problem. We first generate a large number of views as candidates to choose from. Each view will cover a number of planes in the prior. Thus we make each view a "set", while the planes that need to be covered form "elements". The optimization objective is to find the minimum number of views that cover all salient planes. Assuming that each view exposes the same dose onto the patient, minimizing the number of projections will then also minimize X-ray dose.

The set-cover problem (SCP) was one of Karp's 21 NP-complete problems [11]. A mathematical model for the SCP is usually described by a 0-1 matrix. *S*. Let $A(a_{ij})$ be an *m*-row, *n*-column, zero–one matrix. We say that a column *j* covers a row *i* if $a_{ij} = 1$. Each column *j* is associated with a nonnegative real cost c_j. Let $I = \{1, \ldots, m\}$ and $J = \{1, \ldots, n\}$ be the row set and column set, respectively. The SCP can be stated as:

$$\min\{\sum_{j=1}^{n}(c_j \cdot x_j)\} \qquad (11)$$

subject to

$$\sum_{j=1}^{n} a_{ij} \cdot x_j \geq 1 \qquad \forall i \in I \qquad (12)$$

$$x_j \in \{0,1\} \qquad \forall j \in J \qquad (13)$$

where $x_j = 1$ if set *j* is selected, otherwise $x_j = 0$.

In order to generate matrix $A(a_{ij})$, we test a large number of projections. If we assume that all projections have the same source-axis and detector-axis distance, the possible projection locations should be on a sphere and can be parameterized by the longitude φ and the latitude λ. Their ability to cover the strong edges in the prior volume is stored in $A(a_{ij})$.

This procedure is computational intensive and makes for the most time consuming part of the framework. We generate the set-cover problem by GPU simulation. Here we illustrate how to test whether one projection will cover a given plane.

The input is the projection geometry, φ and λ and a point **p**, which uniquely define a plane. A projection has width *w* and height *h*. Output will be 1 for "cover" and 0 otherwise.

The projection will cover the plane if, and only if, there exists a ray that satisfies the two following conditions:

1. The viewing ray is orthogonal to the plane's normal.
$$\mathbf{p} \cdot \mathbf{d}_{view} = 0 \qquad (14)$$
2. The viewing ray hits the plane's center (the point defined by **p**).
$$\frac{\mathbf{p}-\mathbf{s}}{|\mathbf{p}-\mathbf{s}|} \cdot \mathbf{d}_{view} = |\mathbf{d}_{view}| \qquad (15)$$

We implemented the computation in CUDA (the programming API for GPUs). The CUDA kernel will launch $w \times h$ threads to test the two conditions in Equations (14, 15). If there is one thread that satisfies the two conditions, the result is written as 1 for "cover".

C. Ant Colony Optimization

SCP can be solved by many algorithms and the ant colony algorithm is one of the fastest solvers [12][13]. It is inspired by the observation of real ant colonies. In SCP, a large amount of artificial ants are searching for an optimal solution defined by equation (11). Each artificial ant chooses a set one by one until it achieves a complete cover defined by equations (12, 13). The probabilities for choosing different sets are partially based on a pricing method. Additionally, the probability for choosing one set will increase if a large amount of ants choose it. See [12][13] for more details of the ant colony optimization for set-covering.

D. Iterative Reconstruction

We use the SART algorithm with GPU-accelerated forward projection and back-projection. As motivated in [5][6], we need to place additional projections around the object if the projections are too few. In this case, we first evenly distribute 36 projections around 360 degrees. Then we replace the projection positions with the nearest of the salient views.

IV. Results

For our experiments, we used a cone-beam simulator with source-axis-distance=1000mm and detector-axis-distance= 5000mm. The detector resolution was set to 1024×768 with pixel size 0.388mm×0.388mm. For the view generation, we sampled 200 projections along the longitude dimension across 360 degrees and sampled 7 projections along the latitude dimension within ±8 degrees. After we obtained favorable views, we applied additional shift to the prior, to test the performance on a different instance of the similar dataset. We used non-local mean filtering in regularization to eliminate streaks in few-view CT reconstructions.

The first experiment is a cube. The prior volume is an 8^3cm cube with shifted 1cm×2cm×3cm from the scanning center. We set the threshold to be 85% maximum value in the feature extraction stage. This resulted in 12 planes and k-means clustering reduced the number of planes to 6 (4 of them are shown in Fig. 3d). The ant system returned 4 views which would cover these 6 planes. We applied a 1cm×1cm×1cm shift to the prior and used the SART algorithm with relaxation factor λ=1.0. Fig. 4 shows the central axial slice of the reconstructed 256^3 volume after 30 iterations. We observed that Fig. 4a (with view optimization) converged to a box but Fig. 4b (with evenly distributed projection) did not. Although the object scanned had a small perturbation from the prior, the cone beam aperture was still able to capture desired edge.

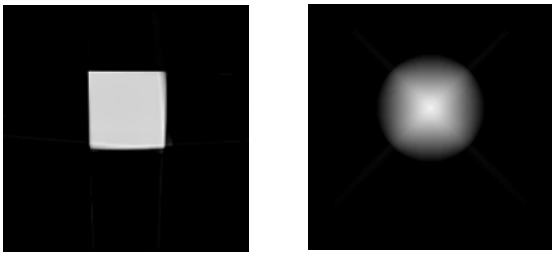

(a) (b)

Figure 4. Reconstructed cube from 4 projections using the SART algorithm (a) with salient views and (b) without salient views.

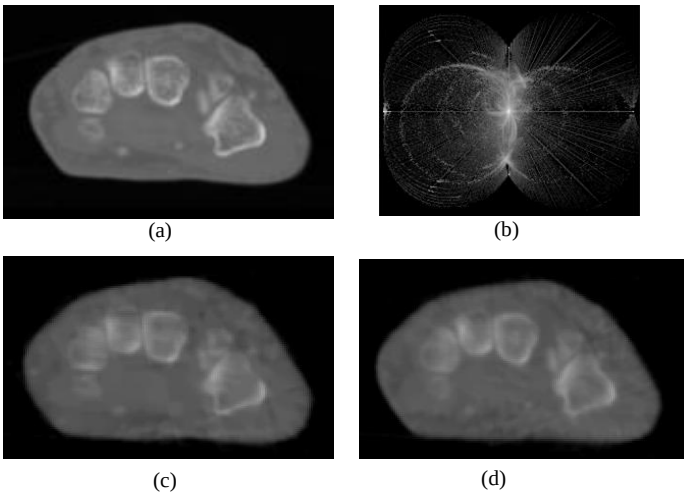

Figure 5. View planning for a hand dataset from 33 projections (showing only central slices). (a) Prior data. (b) Feature space. (c) Reconstruction with view optimization. (d) Reconstruction without view optimization.

Our next example is a hand dataset (Fig. 5). Fig. 5a shows the center axial slice of the prior data. Fig. 5b shows the center (axial) plane of the feature space. The pattern reveals that the dataset has strong horizontal and diagonal edges. We set the threshold to be the 70% maximum value in the feature extraction stage. This resulted in 118 planes, reduced to 100 with the k-means clustering. The ant system returned 33 views. We applied 0.5cm×0.5cm×0.5cm shift to the prior and used SART with λ=0.2. Figure 5 shows the corresponding slice of the reconstructed 256^3 volume after 30 iterations. We observe that Fig. 5c (with view optimization) shows sharper bone boundaries than Fig. 5d (with evenly distributed projections).

The final example is a neck dataset (Fig. 6a) which was extracted from the NIH visible human dataset. The central slice of the feature space is shown in Fig. 6b. The threshold was set to 70% which resulted in 245 planes, reduced to 200 by the k-means. The ant system returned 28 views. We applied a 0.5cm×0.5cm×0.5cm shift to the prior and then applied 50 iteration of SART with λ=0.2. We see that view optimization (Fig. 6c) can resolve details better (see the blobby structure in the center), with reduced streak artifacts and more sharpness.

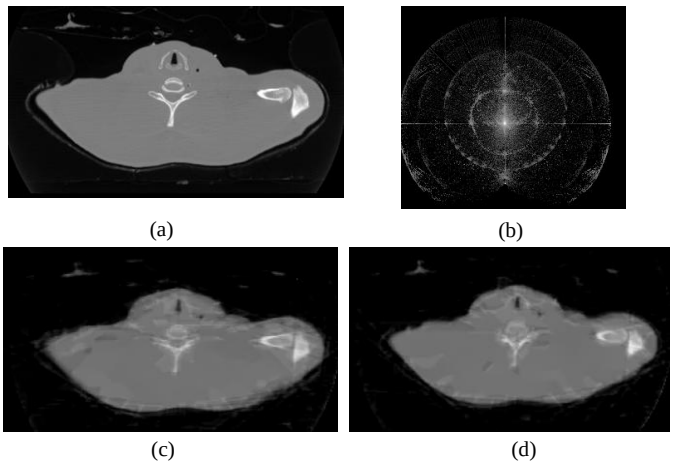

Figure 6. View planning for a neck dataset from 28 projections (showing only central slices). (a) Prior data. (b) Feature space. (c) Reconstruction with view optimization. (d) Reconstruction without view optimization.

All of our experiments were conducted on an NVIDIA GTX 480 GPU, programmed with CUDA 3.2 runtime API and with an Intel Core 2 Duo CPU @ 2.66GHz. Table I show the performance of the different stages of our framework. The most time consuming part is the SCP generation which would be even slower without GPU acceleration.

TABLE I
PERFORMANCE (SECONDS)

Dataset	Radon/Hough transform	K-mean clustering	SCP generation	Ant Colony Optimization
Cube	15	0.01	5	0.01
Hand	16	2	72	11
Neck	16	3	53	9

V. CONCLUSIONS

We have proposed an efficient framework to optimize the total number of projections for iterative CT reconstruction, using prior object information to generate salient views. Our initial results show that our view selection algorithm is quite effective especially when the object has unevenly distributed strong edges. The framework is also more effective when the object scanner's shape and position are closer to the prior volume.

In future work, we would like to employ regularization [2][3] to further improve the quality of the reconstructions. We also plan to implement the ant colony optimization on the GPU, for faster processing. Finally, we plan to use deformable registration to apply some advanced prior knowledge to the CT reconstruction.

REFERENCES

[1] L. A. Feldkamp, L. C. Davis, and J. W. Kress, "Practical cone-beam algorithm," J. Opt. Soc. Am. Vol 1, No. A6, 612–619 , 1984

[2] E.Y. Sidky, X. Pan, "Image reconstruction in circular cone-beam computed tomography by constrained, total-variation minimization," Physics in Medicine and Biology, vol. 53, pp. 4777-4807, 2008

[3] H. Yu, G. Wang, "SART-Type image reconstruction from a limited number of projections with the sparsity constraint," International Journal of Biomedical Imaging, 2010.

[4] W. Xu, K. Mueller, "A performance-driven study of regularization methods for GPU-accelerated iterative CT," Workshop on High Performance Image Reconstruction (HPIR), 2009.

[5] C. Sorzano , R. Marabini , N. Boisset , E. Rietzel, R. Schroder, G. Herman, J. Carazo, "The effect of overabundant projection directions on 3D reconstruction algorithms," J. Struct. Biol, 113, 108—118, 2001

[6] G. Herman, R. Davidi, "Image reconstruction from a small number of projections," Inverse Problems, 24(4):45011–45028, 2008.

[7] W. Scott, G. Roth, J. Rivest, "View planning for automated three-dimensional object reconstruction and inspection," ACM Comput. Surveys 35 (1):64–96, 2003.

[8] E. Quinto, "Singularities of the X-ray transform and limited data tomography in R2 and R3," SIAM J. Math. Anal., 24:1215–25, 1993.

[9] M. van Ginkel , C. Hendriks, L. van Vliet. "A short introduction to the Radon and Hough transforms and how they relate to each other," Technical Report QI-2004-01, Delft University of Technology, 2004.

[10] T. Kanungo, D. Mount, N. Netanyahu, C. Piatko, R. Silverman, A. Wu, "An efficient k-means clustering algorithm: analysis and implementation," IEEE Trans. PAMI, 24:881-892, 2002.

[11] R. Karp. "Reducibility among combinatorial problems". Complexity of Computer Computations. pp. 85–103.1972

[12] M. Rahoual, R. Hadji, V. Bachelet, "Parallel ant system for the set covering problem," Ant Algs, Springer Lect. Notes, 2463:249-297, 2002.

[13] Z. Ren, Z. Feng, L. Ke, Z. Zhang, "New ideas for applying ant colony optimization to the set covering problem," Computers & Industrial Engineering, 58(4):774-784, 2010.